Geothermics 75 (2018) 208–219

Contents lists available at ScienceDirect

Geothermics

journal homepage: www.elsevier.com/locate/geothermics

Scenario analysis on operational productivity for target EGS reservoir in I-lan area, Taiwan

Chi-wen Yu[a], Shih-chang Lei[a], Chih-hao Yang[a,*], Wen-shan Chen[b], Sheng-rong Song[b]

[a] Sinotech Engineering Consultants, Inc., Taiwan
[b] Department of Geoscience, National Taiwan University, Taiwan

ARTICLE INFO

Keywords:
Scenarios analysis
I-lan geothermal site
TOUGH2-EGS
Heat production scenario

ABSTRACT

A basic production scenario analysis (BPSA) using the TOUGH2 code (coupled with a fit-for-purpose modified EGS module) as a relevant simulator was conducted to study a potential geothermal site in I-lan Triangle, Taiwan. The outcome of numerical simulation shows that the capability of the code is compliant with heat production model analysis under a pair of recharging and production wells. In the BPSA application, the model was constituted with an assumed size of 2 km × 2 km × 2.5 km, taking into consideration a relevant boundary condition and using Case-A, B, and C to represent varied depths of recharging points. Heat production histories of target reservoirs containing a fault zone were simulated using a deterministic approach, and a collection of 30-year heat production P/T histories was obtained for all 3 cases. The effects of a fault zone near the production point are evaluated and found to be significant only when distance between the fault's boundary and production point is minimum. The study also shows that relative locations of the recharging point from production point are important to reach an adequate design of production well layout in a geothermal plant. Significant temperature decline can be observed in Case-C of BPSA, where the distance between R-1 and P-1 is the least among the 3 cases studied. Results of this study would provide a useful numerical tool for evaluating future EGS development projects in Taiwan. By adopting a suitable conceptual model and a group of carefully selected relevant parameters, site-specific reservoir engineering problems associated with the recharging and production operation in a representative EGS geothermal field can be foreseen and predicted in a quantitative way.

1. Introduction

To combat global warming and decrease the dependency on fossil fuel, the development of renewable energy and low carbon energy technologies are increasingly important around the world in recent years. Enhanced Geothermal Systems (EGS), which utilize heat generated from elevated thermal gradient, are regarded as a robust energy source for power generation (Tester et al., 2006; International Geothermal Association, 2010; Department of Energy, 2008a,b; Giardini, 2009; Goldstein et al., 2011). In Taiwan, the EGS development plan is a component of the carbon reduction policy implemented on a national scale in Taiwan since the establishment of the National Energy Developing Program (NEP) in 2009. The Department of Geology at National Taiwan University (NTU) had been commissioned by the Ministry of Science and Technology (MOST) as the research principal investigator (PI) of the EGS program since the initial phase up to the present day. Under the supervision of MOST, in a two-phase development, including the first phase (NEP-I) during 2013–2014 and second phase (NEP-II) during 2014–2016, exploration activities covering the preferred EGS sites had been extensively conducted within I-lan County in Northeastern Taiwan. In addition to on-site exploration works, reservoir engineering studies (Ho et al., 2014; Chen, 2016) on physical and chemical properties of rocks in thermal reservoirs (Lyu et al., 2014a,b; Yang et al., 2015), heat flow simulation and capacity building analysis of the EGS reservoir (Lyu et al., 2014a,b), innovative well pressure and temperature measurement devices (Yu and Lei, 2015), as well as many other relevant technologies were developed to assist in the commissioned development plan.

At NTU's request, the research team was organized and was responsible for conducting a preliminary study via reservoir simulation of a potential EGS site. The main task aims at establishing a feasible production capacity estimation analysis procedure and intends to create a competent simulator for application to any potential EGS reservoir in Taiwan. For such an application, analysis of heat exchange behavior of

Abbreviations: BPSA, basic production scenarios analysis; mBGL, meter below ground level; UI, user interface; MP, massively parallel computing; QA, Quaternary alluvium sediment; LS, Miocene Slate Formation; KK, Oligocene argillite; SL, Oligocene quartzite; XT, Eocene slate; TNA, pre-tertiary schistose tectonic basement

* Corresponding author.
E-mail address: yangch@sinotech.org.tw (C.-h. Yang).

https://doi.org/10.1016/j.geothermics.2018.05.003
Received 11 July 2017; Received in revised form 15 May 2018; Accepted 17 May 2018

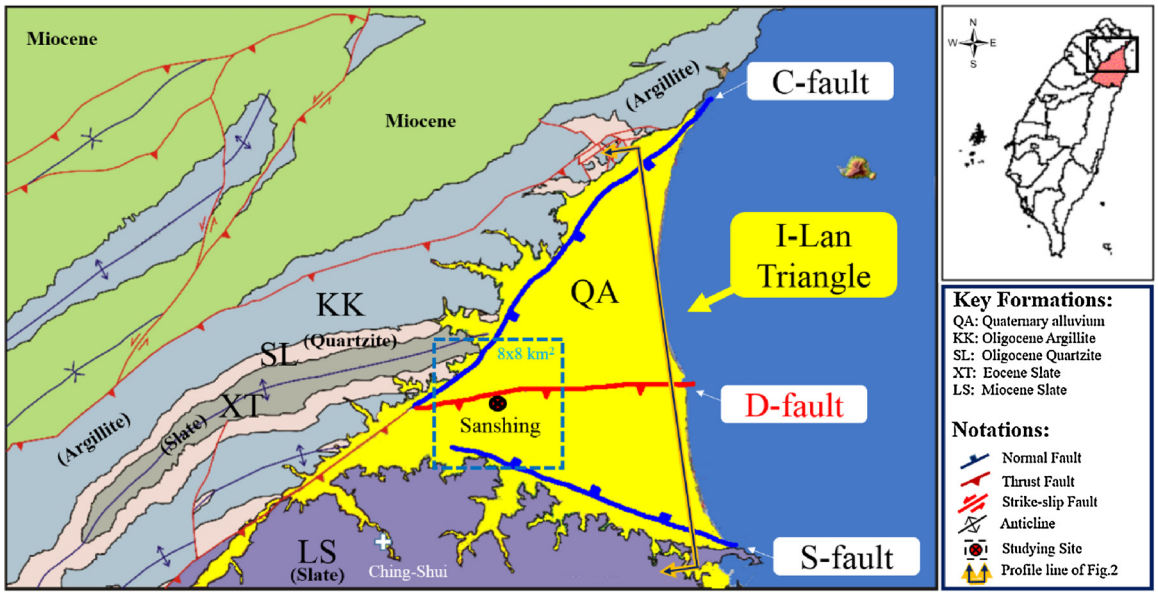

Fig. 1. Geological Map of Surrounding Area of I-lan Triangle (Area in red color in upper-right map indicates I-lan County jurisdiction). (For interpretation of the references to colour in this figure legend, the reader is referred to the web version of this article.)

deep geothermal wells, thermal capacity and deficit assessment can be carried out by means of numerical simulation approaches, and relevant potential of heat production plan can be presented in graphical form prior to engineering design in upcoming years.

It can be noted that high-quality numerical analysis can significantly reduce the cost of unplanned engineering works due to unexpected situations. In addition, possible engineering problems that may occur during underground injection operation in candidate sites can be resolved in a quantitative way. Results of this study would provide a good example for formulating a THM coupling simulation approach that hopefully can provide a useful numerical tool for future EGS project applications in Taiwan.

2. Project background

2.1. Geology of target reservoir

Fig. 1 shows the geological map of the I-lan Plain. The plain, located within I-lan County, forms a triangle-shaped area (I-lan Triangle). Please note that in the vicinity of the I-lan Triangle, three major regional faults are identified, namely (1) C-Fault in the North, (2) S-Fault in the South, and (3) D-Fault in between. Both the C-Fault and S-Fault are believed to originate as tectonic faults derived from Philippine Sea Plate subduction, while D-Fault is a graben fault that formed as a result of the recent opening of the Okinawa Trough.

Due to the active tectonic setting, wide spread natural hot springs and high surface heat flow had been noticed and there have been extensive geothermal exploration studies conducted over the past five decades (Teng et al., 2013). Moreover, a 3-MWe capacity geothermal power plant was constructed in 1981, but retired in 1993 due to insufficient production well flow rates at the Ching-Shui Site; a rapid decline was interpreted to being caused by carbonate scaling (Lee et al., 2012; Zhang et al., 2016).

In recent years, to fill the energy supply gap due to central government's zero-nuclear policy, resuming geothermal development is listed as one of the renewable energy options. The I-lan Plain has been evaluated as one of the most potential sites for developing geothermal plants for power generation. Due to the high geothermal gradient as revealed by abundant temperature survey data, the I-lan Triangle is recommended as an excellent EGS developing site. Fig. 2 shows the speculative geological profile (N-S) of coastal I-lan Plain. As illustrated in the figure, the basement rock formation in I-lan Triangle is overlain by a thick (several meters to several hundred meters) layer of Quaternary alluvium sediment (QA). Slate Formation (LS) occurs on the south flank of D-fault, and Oligocene argillite (KK) and quartzite (SL) and Eocene slate (XT) are present on the north flank. The tectonic basement is composed of a schistose basement formation (TNA) that is Pre-Tertiary in age.

2.2. Conceptual model

Fig. 3 shows the conceptual geological model for the potential EGS resource located in the Sanshing area within the I-lan Triangle. This meshed model is composed of 288,000 elements, covering an on-site 3-D dimension of 8 km × 8 km × 3 km, using the model grid generating tool developed by the authors. Here, the model top is the surface topography, and the bottom elevation reaches to 3000 mBGL (i.e., meters below ground level). Local geological investigation had reported that under the thick top alluvium deposit, the major formations in the model were KK, SL, XT (from top to down) with formation thicknesses of 450m, 1,550m, and 500m, respectively. On the left side of the model, the massive LS (slate formation) fully ***occupies*** the south foot wall of D-fault *with limited overburden of QA*. The C-fault and D-fault in the model are defined in both Figs. 1 and 2. In general, these faults are interpreted as normal faults in the model. By evidence of some local geological investigation (e.g. Teng et al., 2013), the model area is regarded as having a high geothermal gradient district worthy of EGS exploration to meet the domestic renewable energy demand. The well location at the model center shown in Fig. 1 is only conjecture, and some research deep wells are under planning by the NEP.

The SL (quartzite formation) in the north flank of D-fault is assumed to be as a good aquifer and a good heat exchange rock layer, because the rock mass was usually found to be highly fractured accompanying tectonic fissures. In the meantime, the D-fault is also regarded as a potential good conduit for fluid convection, although this needs to be confirmed. The KK (argillite formation) is assumed to play an important role as a cap rock which prevents the escape of abundant underground heat. From a technical point of view, the I-lan Triangle has its well defined reservoir nature suitable for developing an EGS site. However, more geothermal data need to be collected, and some validating deep exploration wells must be drilled in the future.

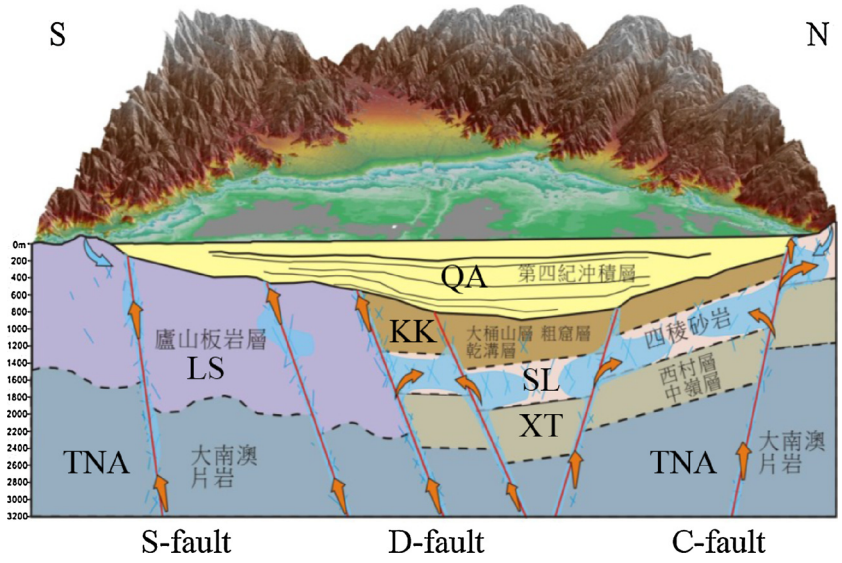

Fig. 2. Speculative Geological Profile (N-S) of I-lan Plain (Profile line see Fig. 1).

3. Heat production simulation

3.1. Simulation tools

The main simulator used in current study is TOUGH2-EGS. It is a novel fully-coupled flow and geo-mechanics model for simulating enhanced geothermal reservoirs (Hu et al., 2013). The pre-existing TOUGH2 code (Pruess et al., 1999; Pruess, 2005) can solve problems associated with the transport of unsaturated groundwater and heat, and has a wide application of functional modules that facilitate simulation of coupled thermal (T) and hydraulic (H) processes. As an extension in its EGS modules, a simulation of thermal-hydrological-mechanical (T-H-M) coupling problems can be further modelled in a numerical manner. It is a practical code improvement because in some energy-related engineering project like EGS project, some design problems such as ground deformation, structural foundation instability, subsurface instability inducing micro-seismicity and/or triggering earthquakes may happen. As a consequence, a simulator with mechanical simulating capability is always necessary. EGS modules allows the integration with TOUGHREACT (Xu et al., 2012), a reactive chemistry analysis module, hence it can be used to simulate a T-H-M-C (thermo-hydro-mechanical and chemical) coupling behavior.

Fig. 4 shows the main flow chart of the data solving process using the TOUGH2 code (Pruess et al., 1999). A functional built-in EOS (equation of state) module can be implemented into the process frame as required. Some improvements have been made by the authors to accommodate the code used in the EGS model of the I-lan Triangle. Improvements aim at:

(1) Developing a relevant irregular mesh generator and optimizing mesh structure for the complex geological and reservoir model in the study. The default Mesh-Maker sometimes cannot fit this purpose,
(2) Compiling the code with a MP (massively parallel computing) version.

As a pre-processor, the flexible use of irregular mesh structure is also implemented in establishing a comprehensive simulation model that can be fully compatible with the TOUGH2-EGS code. The benefit of using an irregular mesh is it saves the redundant mesh number for insensitive zones, and speeds up the overall calculating time in the modelling process, especially when the close-up of near field behavior

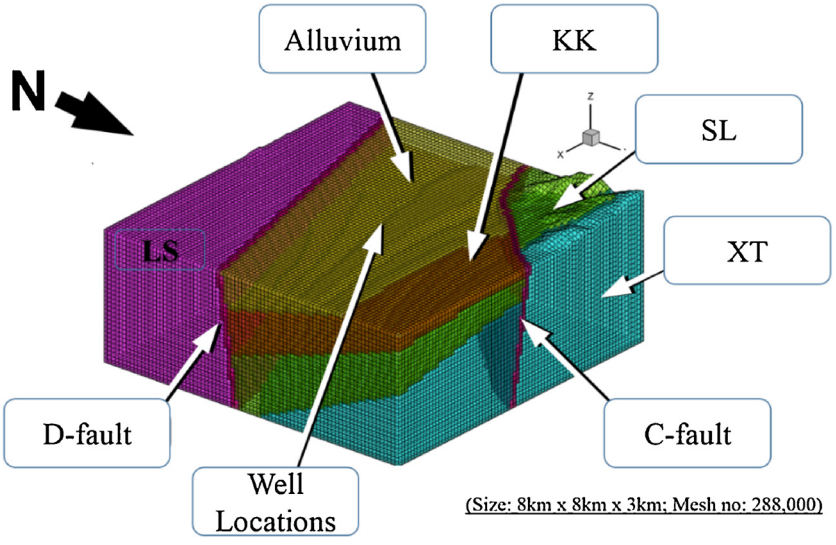

Fig. 3. Localized Geological Model of Geothermal Plan within the **I-lan Triangle.**

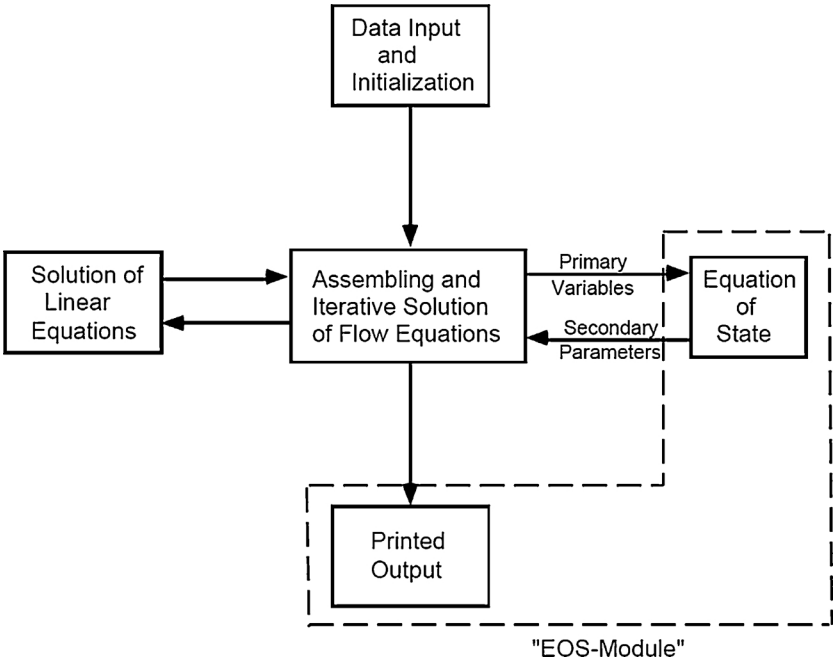

Fig. 4. Flow Chart of Data Solving Process in TOUGH2 (After Pruess et al., 1999).

of a production well is needed.

The original MP-version of the TOUGH2-EGS code was provided by the Colorado School of Mines (Perapon et al., 2013); it was written on a Linux operational system platform. For studying convenience, Linux system was switched to the commonly used Windows® system, and a modified version was developed. Table 1 summarizes the major changes which were done in our study, and some of notable changes are listed as below:

(1) Expanding functions of existing pre- and post- processors,
(2) Re-compiling the modified TOUGH2-EGS for current study,
(3) Re-building new user interface (UI) for the simulators.

As an example shown in Fig. 5, by combining existing survey data, the geological information can be integrated by the developed user interface (UI) as a pre-processor tool to assist in the generation of the conceptual geological structure model. Our study had completed the compilation of the parallel computing (MP) program under the Windows® system from original Linux system, which can carry out multi-core processing. Although it is still incapable of performing a cross-machine operation (e.g., PC clusters), the running efficiency of the current mode has significantly improved than merely on a single PC.

Table 1
Major Changes in Modified TOUGH2-EGS MP Version.

Target Parameters	TOUGH2-EGS (Perapon et al., 2013)			
	Single PC Version		MP Version	
	Original	This Study	Original	This Study
(1) Non-orthogonal Irregular Mesh Generation[a]	N	Y	N	Y
(2) General Output	Y	Y	Y	Y
(3) Output of Element Center	N	Y	N	Y
(4) Output of Element Connecting Vector	N	Y	N	Y
(5) Ionic Output of Element	N	Y	–	–
(6) Mineral Output of Element	N	Y	–	–

[a] Improvements of mesh generation are only in the pre-processor.

3.2. Basic production scenario analysis (BPSA)

A feasibility study on developing a conceptual 5-MWe heat production and geothermal power generation plant in the Sanshing area within the I-lan Triangle was submitted by Jet Yen Company (2012). The study had a hypothetical drilling site. Through the use of some very rough early estimates, the designed input parameters for such a power generation plant associated with the above model region of interest are summarized and listed in Table 2. These design data served as a reference case for planning the basic production scenario analysis (BPSA Case). Due to the unclear reservoir rock situation, a total of three possible scenario cases (Case-A, B, C) were considered in the heat production scheme to cover possible variations in production cases. All these imaginary reservoir cases considered in the heat production plant are illustrated in Table 3 and the production well arrangement shown in Fig. 6. In this BPSA study, the major changing factor of the production scenario is to consider the injection point (I-1) under three different depth levels at 1200 mBGL (Case-A), 2000 mBGL (Case-B), and 2500 mBGL (Case-C) respectively, against a constant production point (P-1) at 3000 mBGL.

Well configurations shown in Fig. 6 might not match the general definition of an EGS plant where the depth and thermal condition of P-1 and R-1 are beyond typical pattern in a strict sense. Nevertheless, to fit in a near field domain containing a steep fault, a reduced model size of 2 km × 2 km × 2.5 km, with a total mesh element number of 80,000 is used for heat production simulation as depicted in Fig. 7. This conceptual geothermal production model includes major geological formations including KK, SL, XT, and a major regional fault (representing D-fault). On average, each mesh cube width is around 50 m. The top and bottom depth scales of the near-field model shown in the figure are 1000 mBGL and 3500 mBGL respectively, without consideration of topographic influence. In the hanging wall of the D-fault (see Fig. 7), the uppermost formation in the model is KK (mainly argillite) with a thickness of 450m, which overlies the SL Formation (mainly quartzite), which has a thickness of 1,550m. Underneath KK and SL is XT Formation (500 m thick, mainly slate). The LS slate formation did not appear in the model and is speculated to lie somewhere under the foot wall of the D-fault. In the model, the D-fault is assumed to have a thickness of 100 m and a high dip angle of 82° toward the North.

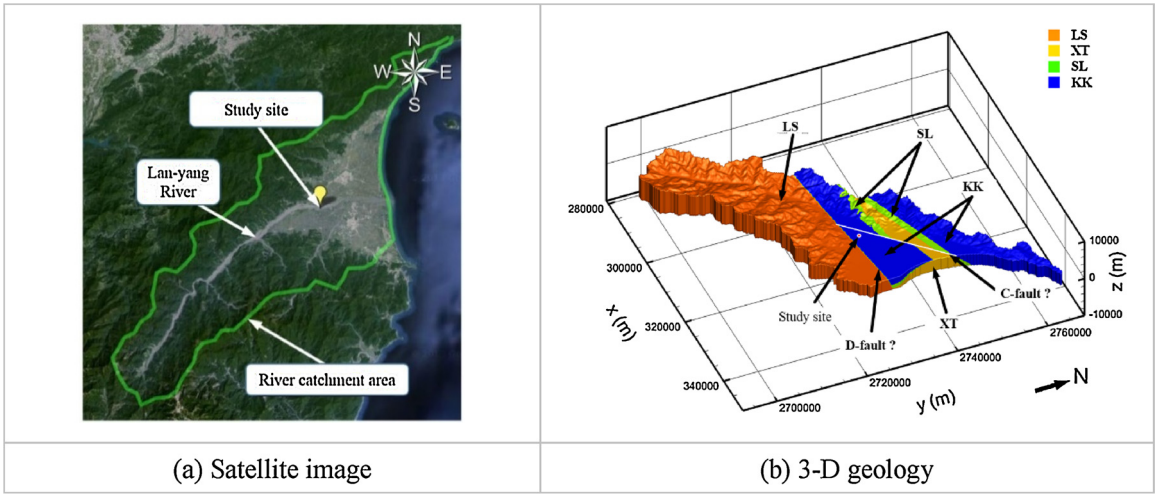

Fig. 5. Generation of Conceptual Geological Structure Model by the Developed Interface.

Table 2
Conceptual Design Data of Heat Production Plant **(BPSA Case)**.

Parameters	Unit	Design Data
1. Circulating cooling water temperature	°C	25
2. Cooling water outlet temperature	°C	36
3. Heat source conditions	°C t/h	N.A.
4. Water inlet temperature (T_i)	°C	120
5. Water outlet temperature (T_o)	°C	80
6. Hot water flow	t/h	1080[a]
7. Input thermal power	MW_t	50.2
8. Output electric power (gross)	MW_e	5.4781
9. Thermal cycle efficiency (gross)	%	10.91
10. Output electric power (net)	MW_e	5.0946
11. Thermal cycle efficiency (net)	%	10.15
12. Internal power consumption	kW	383.5
13. Condenser cooling water flow	t/h	3500
14. Installed power capacity	MW	5.6

[a] Denoting group well conditions; hot flow output per single well requires at least 150 t/h (41.7 kg/s).

The schematic layout of the two-well model is illustrated in Fig. 7 together with its given boundary condition in a BPSA using TOUGH-EGS. The boundary condition of used model is described briefly as follows:

(1) At the model top (1000 mBGL): a fixed boundary initialized with P_{top} = 10 MPa, T_{top} = 80 °C; in the fixed state boundary, water and heat can flow in and out at the fixed mesh element at a constant P and T;
(2) At the model bottom (3500 mBGL): a fixed boundary initialized with P_{bot} = 35 MPa, T_{bot} = 140 °C. Here a constant heat flow bottom boundary representing an underlying heat source was not used because no reliable heat flow (flux) data are available in the I-lan site at this point;
(3) No flow boundary at four sides;
(4) Re-charging point (R-1): constant flow rate (41.7 kg/s) boundary at 1200, 2000, and 2500 mBGL respectively, the designed water outlet temperature (T_r) is 80 °C;
(5) Production point (P-1): constant flow rate (41.7 kg/s) boundary at 3000 mBGL, the designed water inlet temperature (T_p) is120 °C.

Non-fixed state boundaries at top and bottom of the model are also tried for the purpose of comparing production simulations for all cases. In the BPSA, typical rock parameter values of the major rock formations and interfering fault zone in the model are assumed and outlined in Table 4. During the heat production process, both the flow production rate (P-1) and recharging or re-injection rates (R-1) are all set at a constant value of 41.7 kg/s (or 150 t/h) to cope with single production well scenario.

4. Simulation results & discussion

4.1. Heat production layouts

Fig. 8 shows the numerical model for an imaginary geothermal reservoir system that has two essential inherent wells configured for Case-A, Case-B, and Case-C. The production point (P-1) is designed in the model center with a depth reaching 3000 mBGL inside the lower SL quartzite. The recharging points (R-1) are assumed to be at changing depths between 1200–2500 mBGL, located respectively inside KK (Case-B) or SL quartzite in upper (Case-B) and middle (Case-C) level. The horizontal distance between the two points remains a constant value at around 100 m. In all BPSA simulation cases, the production and recharging points are assumed to be located in the hanging wall of the North-dipping normal type D-fault.

In line with the boundary condition mentioned above, two sets of simulations were classified and hereby named as (1) “Set-1 fixed state”, and (2) “Set-2 non-fixed state”. In “Set-1 fixed state”, the simulation was carried out with its boundary conditions, fixed top, no flow side, and fixed bottom. After running for a long time, then start production with the same boundary conditions. Whereas in “Set-2 non-fixed state”, with its boundary conditions for all sides were no flow case, and hydrostatic and conductive temperature were preset. During the

Table 3
Imaginary Reservoir Cases Considered in the Heat Production Plant.

Case ID	Production Well (P-1) Depth (km)	Recharging Well (R-1) Depth (km)	Production Inlet (P-1) Flow Rate (kg/s)[t/day]	Recharging Outlet (R-1) Flow Rate (kg/s) [t/day]	Vertical Depth Diff. (km)	Bedding Dip Angle (degree)	Fault Existing? (Y/N)
A	3	1.2	(41.7) (150)	41.7 (150)	1.8	6	Y
B	3	2.0	(41.7) (150)	41.7 (150)	1.0	6	Y
C	3	2.5	(41.7) (150)	41.7 (150)	0.5	6	Y

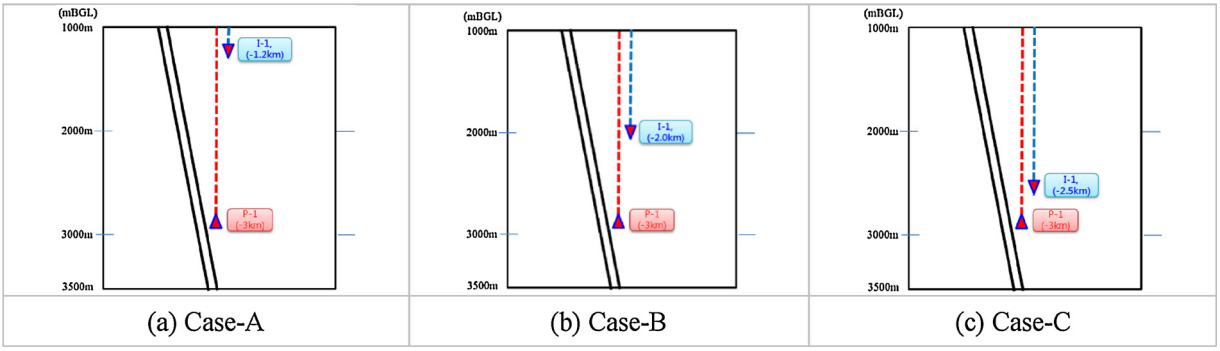

Fig. 6. Reservoir Structures of the Heat Production Models in BPSA Case.

production time of Set-2 simulation, the top, side and bottom remains closed. In both sets, the full numerical domains were initialized as constant temperature fields reflecting a vertical gradient around 24 °C/km, and a hydrostatic pressure field. Fig. 9 shows the initial P-T conditions prior to the heat production simulation respectively for Case-A, Case-B, and Case-C in fixed state boundary case. In general, steady state stability conditions were reached respectively for all simulation cases. This can be achieved by running the simulation with boundary conditions for a long and relevant time. Table 5 shows the start-up P-T values of the simulation model prior to heat production simulation.

Prior to the heat production simulation, the initialized P-T conditions shown in Fig. 9 played as start-up P-T conditions (initial conditions) for all the heat production simulation cases. During the heat production simulation, the cool flow injects into the model at the outlet of R-1, and heated mass flow can flow into the inlet of P-1. Here, the influences of relative location of the R-1 and P-1, and the adjacent fault zone are compared in the heat production study. In all cases, the operation life-cycle of heat production time of the lower temperature modelling reservoir is assumed to be 30 years. During the heat production simulation, cool mass flows in the set-up R-1 re-injection points (Case-A in KK argillite, and Case-B, C in SL quartzite) will migrate along certain paths which run across the quartzite reservoir with an intruding fault zone, prior to entering into the production inlet P-1 (in SL quartzite at 3000 mBGL). The production scenario in terms of pressure and temperature evolutions in the recharging and production points within the geothermal reservoir containing a nearby fault zone can thus be analyzed, and the results are discussed below.

Table 4
Values of rock parameters of major rock formations in the model.

Parameters Selected	QA	KK	SL	XT	LS (Slate)	Fault Zone
Density (kg/m^3)[a]	1800	2680	2640	2600	2780	2600
Porosity	0.3	0.03	0.04	0.04	0.012	0.1
Permeability (Darcy[b])/ Rock mass	1	0.01	1.86*	0.01	1*	2*
Thermal Conductivity (W/m-°K)	2.5	3.4	4.4	3.0	3.2	3.0
Specific Heat (J/kg-°K)	2.5	3.4	4.4	3.0	3.2	3.0

[a] Denoting bulk rock mass condition (including rock discontinuities), very low matrix permeability.
[b] One Darcy is approximately equal to 10^{-12} m^2.

4.2. Pressure and temperature distributions at various production times

At the end of 30 years, the simulated pressure and temperature (P/T) distributions versus production time, are illustrated in Figs. 10 and 11, which show major disturbances near production and recharging points within the entire model domain. In the pressure domain (P-domain), no significant changes can be observed for all cases. From the

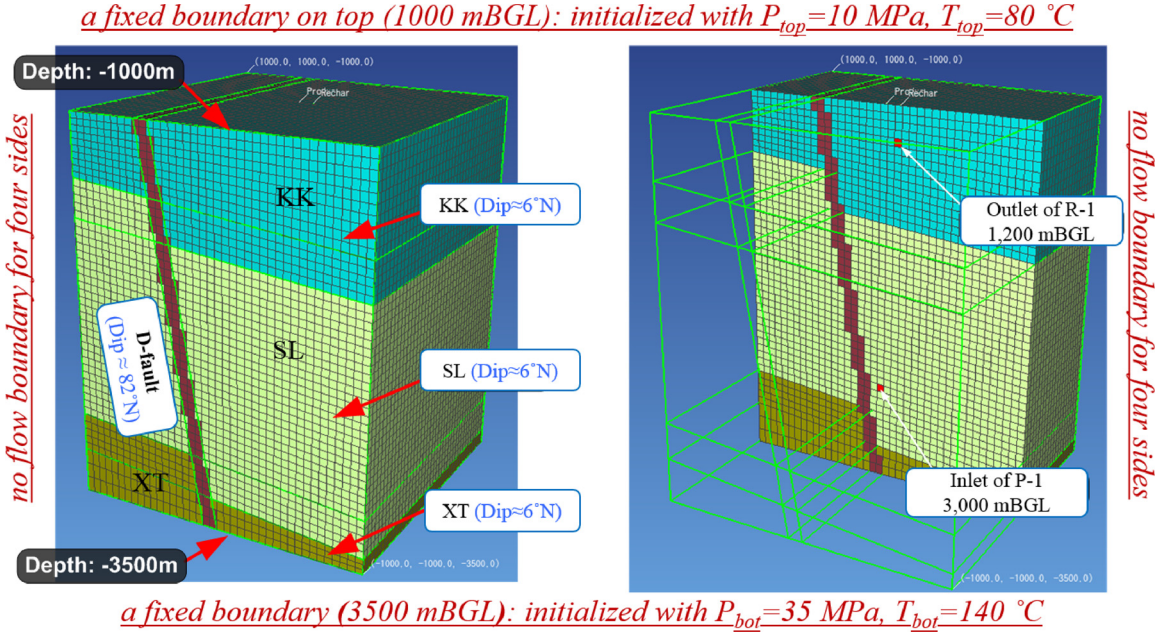

Fig. 7. Schematic Layout of Heat Production Model and Well Arrangement.

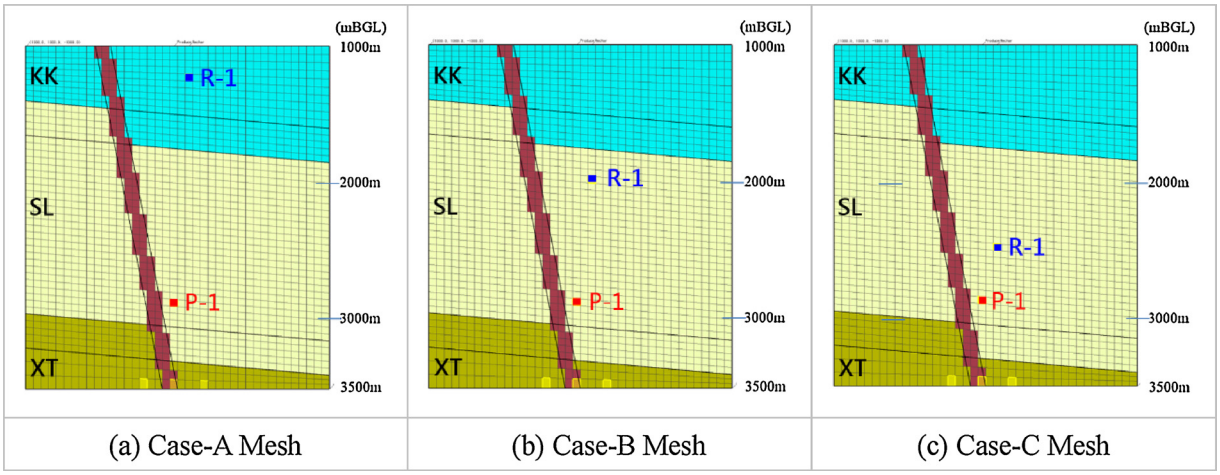

Fig. 8. Schematic Layout of Heat Production Model.

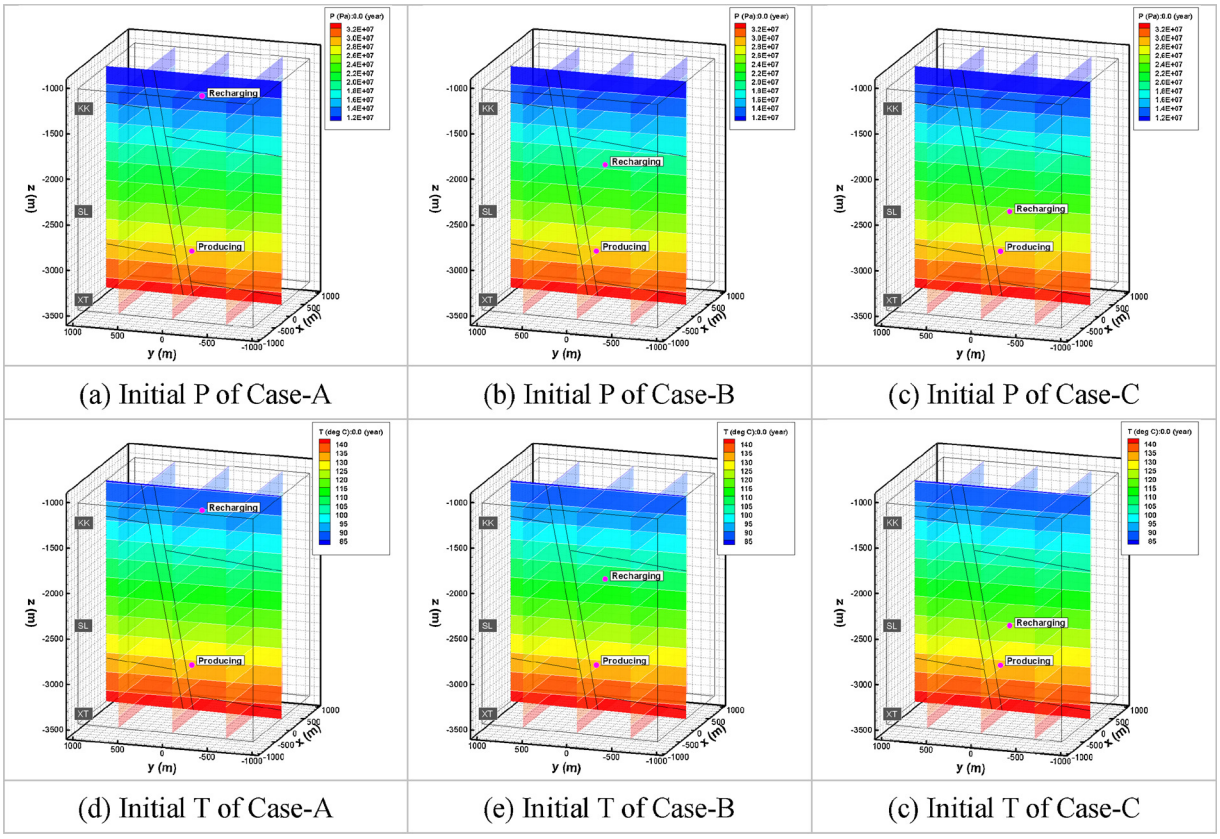

Fig. 9. Initial P-T Conditions Prior to the Heat Production Simulation.

Table 5
Initial P-T Values Prior to Heat Production Simulation.

Model	Input Top P/T (MPa/ °C)	Input Bottom P/ T (MPa/ °C)	Pressure at P-1 (MPa)	Pressure at R-1 (MPa)	Temp. at P-1 (°C)	Temp. at R-1 (°C)
Case-A	10/80	35/140	27.6[a]	12.1[a]	128.9[a]	89.5[a]
Case-B	10/80	35/140	27.6[a]	19.2[a]	128.9[a]	107.6[a]
Case-C	10/80	35/140	27.6[a]	24.0[a]	128.9[a]	119.6[a]

[a] Value denoting P or T at center of zone element within the model.

model top to bottom, the pressures are constantly stable and consistent with the hydrostatic pressure. Some slight change will be discussed in the following section. In contrast, in the temperature domain (T-domain), significant changes can be observed with the locations of different levels of R-1. The signatures of cool water can be noted around R-1 outlet points. At the end of 30 years, near the outlet of R-1, all temperatures are all approaching to the designed water outlet temperature (T_o = 80 °C) shown in Table 2.

The stabilizing start-up temperature (128.9 °C) of P-1, prior to heat production, is close to 130 °C under the given boundary condition, which is slightly higher than the designed water inlet temperature (T_i = 120 °C, see Table 2). Due to the heat production, the temperature at P-1 will decrease with the withdrawal of heat from the reservoir. To

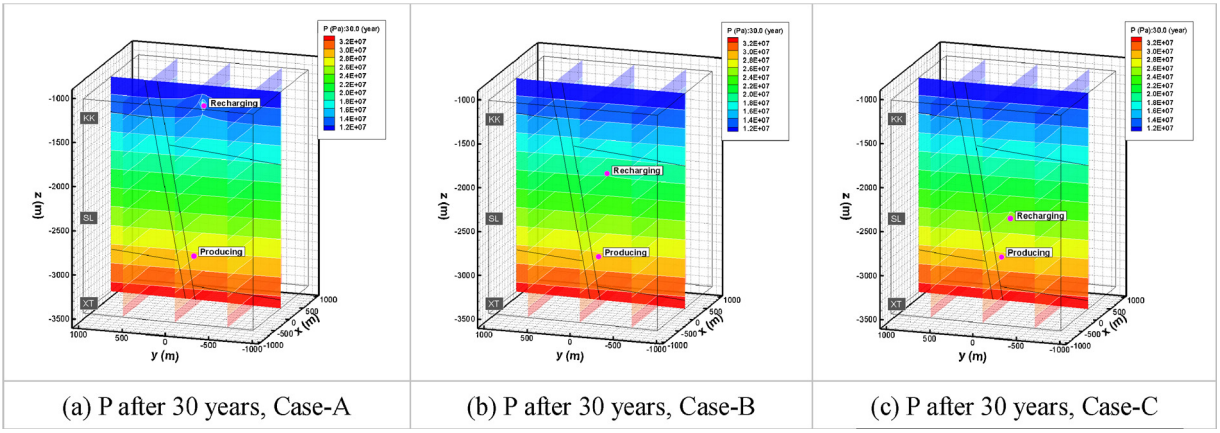

(a) P after 30 years, Case-A (b) P after 30 years, Case-B (c) P after 30 years, Case-C

Fig. 10. Pressure Distributions Modelled at 30-year Production Times.

maintain the constant heat supply, a constant geothermal heat source from the deeper part (i.e., fixed state bottom boundary in this study) is essential. The supply can also be partly contributed by the nearby D-fault, due to its high heat transfer capability. In Fig. 11, upward heat perturbations can be observed and run across the adjacent fault zone inside the model domain.

In the process of recharging and production, the low temperature from R-1 can affect the production temperature at P-1 only when they are close to each other, as in the cases of Case-B and Case-C. In Case-A as shown in Fig. 10(a), the R-1 is located in the low permeability KK-argillite and keeps a vertical distance away from P-1 by 1.8 km, such that the cool water does not noticeably affect the production temperature. In such case, the heat supply will be quite isolated with the recharging influence.

Due to the very close distance of fault zone to the P-1 inlet, the "fault zone effect" plays quite an important role in circulating the heat to production point P-1 (see Fig. 11). Especially when the rock permeability parameter values of the fault zone (2 Darcy) are assumed to be a bit higher than those of reservoir rocks (1.86 Darcy for SL quartzite). The circulation of heat flow adjacent to the fault zone will be enhanced if the permeability of fault zone is increased.

4.3. Time lapse P-T evolutions during the heat production process

(1) Pressure Evolution

Before the heat production, the start-up fluid pressure and temperatures at recharging point R-1 and production point P-1 had been outlined in Table 5 and indicated in each plot. In general, the start-up pressure values of the R-1 and P-1 were approximately identical to the hydrostatic pressure for each point within the model domain. Fig. 12 shows the results of pressure (P) evolutions (solid lines for fixed state cases) during the 30-year heat production period respectively for Case-A, B, and C.

At the recharging point R-1, the pressure tends to increase due to the injection of cool water, whereas in the production point P-1, the pressure tends to decrease due to hot fluid withdrawal. For Case-A in Fig. 12(a), the reservoir pressure in recharging point R-1 increases from 12.1 to 19.3 MPa in recharging point R-1 over a very short time (i.e., within one year), and then remains at a relatively stable pressure level until the end of production. The great pressure increase in the outlet of R-1 can be explained by the low permeability of the rock in KK argillite. In Fig. 12(b) and (c), the results of the reservoir pressure change in recharging point R-1 were not significant for Case-B (19.2–20.0 MPa) and Case-C (24–24.7 MPa). The limited pressure increases in the outlet of R-1 can be explained by the high permeability of the rock in SL quartzite. Both of their reservoir pressures became quite stable over a very short time, exhibiting similar pressure responses as that of Case-A. As for the production inlet at P-1 within SL quartzite reservoir, basically for all simulation cases, there were only minor pressure changes observed at the production point P-1, where all dropped from approximately 27.6–26.7 MPa (less than 1% only).

All the plots shown in Fig. 12 were compared against the results of P-evolutions at R-1 and P-1 points with a non-fixed state top/bottom boundary (i.e., dashed lines). The time lapsed temperatures in non-fixed state case show a slightly lower trend but the difference with the fixed state case (i.e., solid lines) can be ignored.

(2) Temperature Evolution

Temperature evolutions in R-1 and P-1 are highly dependent on the

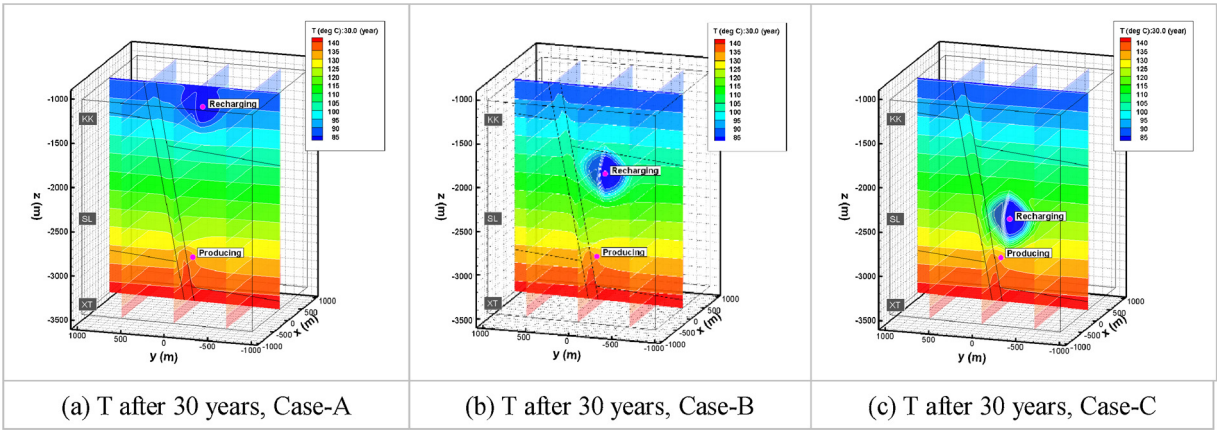

(a) T after 30 years, Case-A (b) T after 30 years, Case-B (c) T after 30 years, Case-C

Fig. 11. Temperature Distributions Modelled at 30-year Production Times.

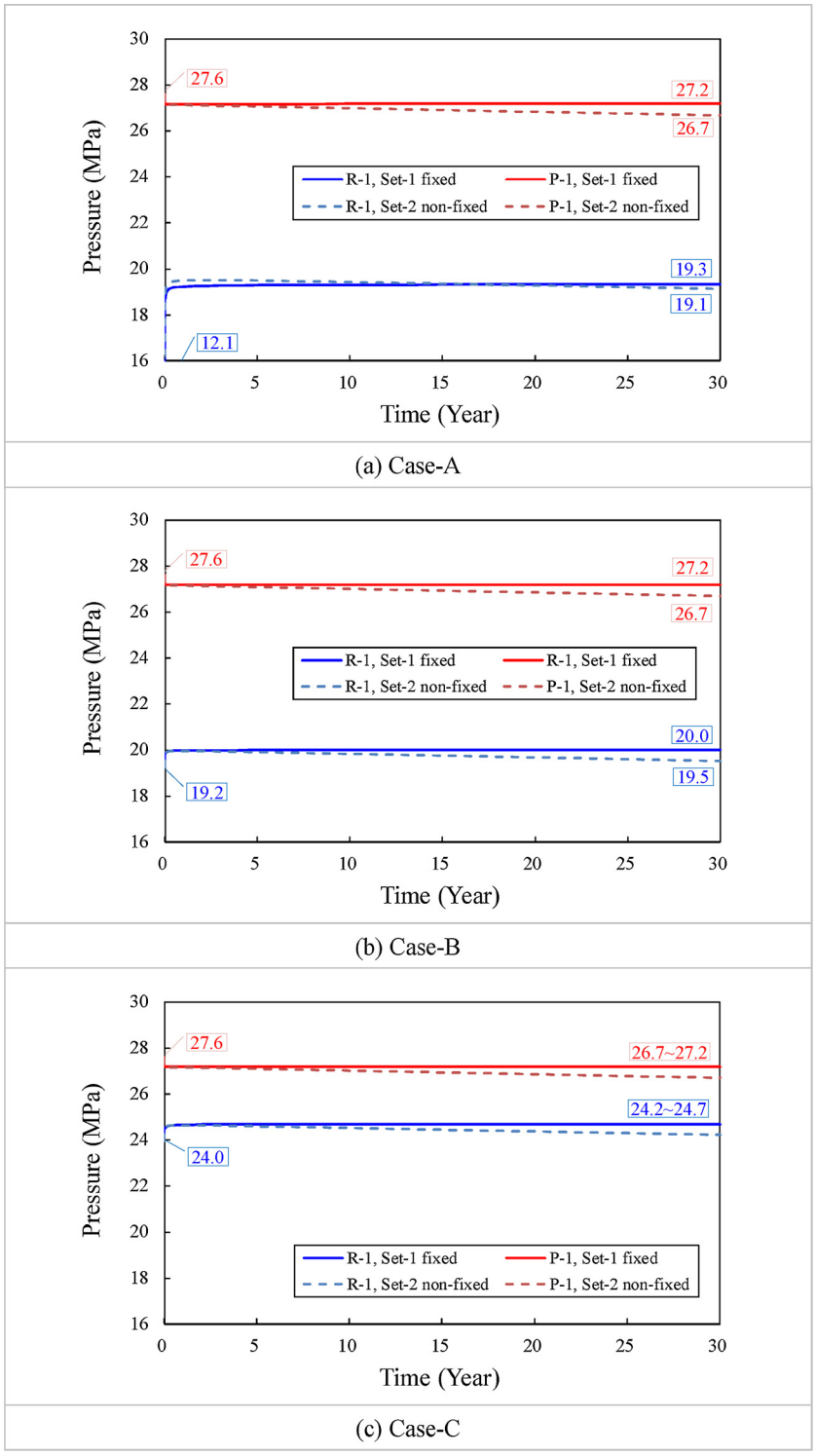

Fig. 12. Pressure Evolutions during the 30-year Heat Production Period.

designed flow rate and temperature at the inlet and outlet zones of a production plan. Fig. 13 shows the results of temperature (T) evolutions during the 30-year heat production period respectively for Case-A, B, and C. The starting fluid temperatures in P-1 encountered in the early production phase is 128.9 °C. Fluid temperatures in R-1 are dependent on the depth for Case-A, B, and C, and at start-up values of 89.5, 107.6, and 119.6 °C. For Case-A in Fig. 13(a), due to the heat production at P-1 during the early production phase, the start-up fluid temperatures in the recharging point (R-1) quickly dropped to the designed injection water outlet temperature (80 °C, see Table 2) and then sustained at a constant level (around 80.0 °C) till the end of production. Correspondingly, at the P-1 point, a trend of temperature increase, from 128.9 °C rising up to 130.1 °C, can be observed in the Case-A plot. This results might not look realistic given that heat is being withdrawn from the system and cooler water is being reinjected.

Nevertheless, the temperature rise in P-1 can be explained by the configuration of the relative locations of P-1 and R-1, and the fault zone. For this case, cool water flow was re-injected into the reservoir

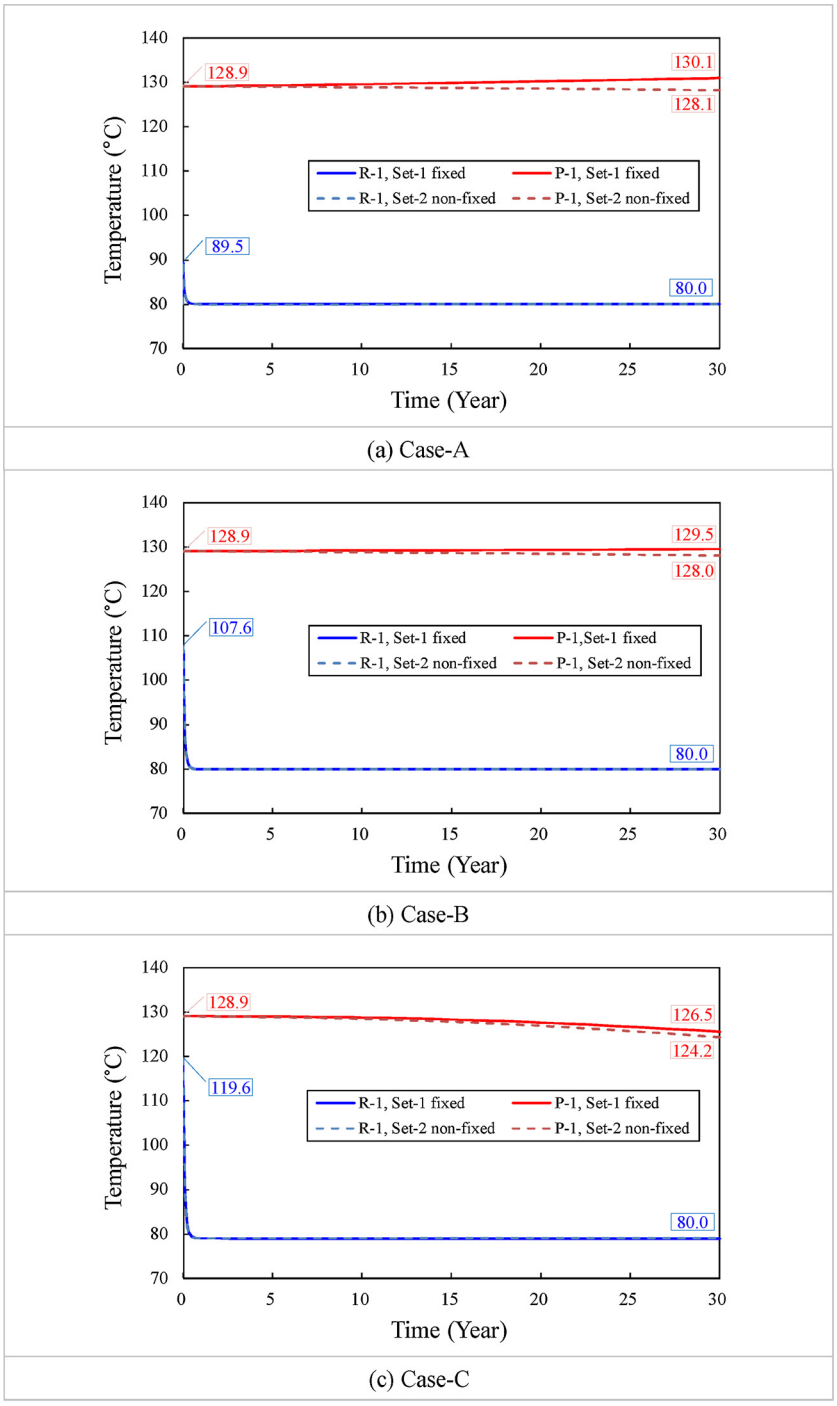

Fig. 13. Temperature Evolutions during the 30-year Heat Production Period.

through the outlet of R-1 at KK formation where the argillaceous rock permeability (0.01 Darcy) is relatively lower than the SL quartzite reservoir (1.86 Darcy). Another contributing factor is that the vertical distance from R-1 to P-1 is as far as 1,800m. Hence it can be expected that the cool water migrating into P-1 will require significant period of time. On the other hand, because the major fault is trending towards the production point (P-1) and fault boundary is within only a short distance from P-1, the heat source from the bottom boundary can thereby supply high rate of heat flow due to fault zone's high permeability (2 Darcy). As a consequence, the heat compensation from the fault zone circulation are apparently much higher than that from cool water re-injecting into R-1, resulting in the gentle temperature rising in Case-A.

When the vertical distance from R-1 to P-1 is reduced, as in the cases of Case-B and Case-C, the influences of cool water from R-1 increased, and the production temperatures in P-1 will gradually decline with production time. A significant trend of temperature reduction can be observed in Case-C (decreased from 128.9 °C down to 126.5 °C), where only 500 m vertical distance from R-1 to P-1 is observed.

Similar to P-evolution discussion mentioned earlier, all the plots shown in Fig. 13 are also compared against the results of T-evolutions at R-1 and P-1 points with a non-fixed state top/bottom boundary (i.e., dashed lines). The eventual temperature rising in P-1 observed in non-fixed state case of Case-A is noted to be insignificant. In general, the time lapsed temperatures in non-fixed state case show a slight lower trend but the difference with the fixed state case (i.e., solid lines) can be ignored.

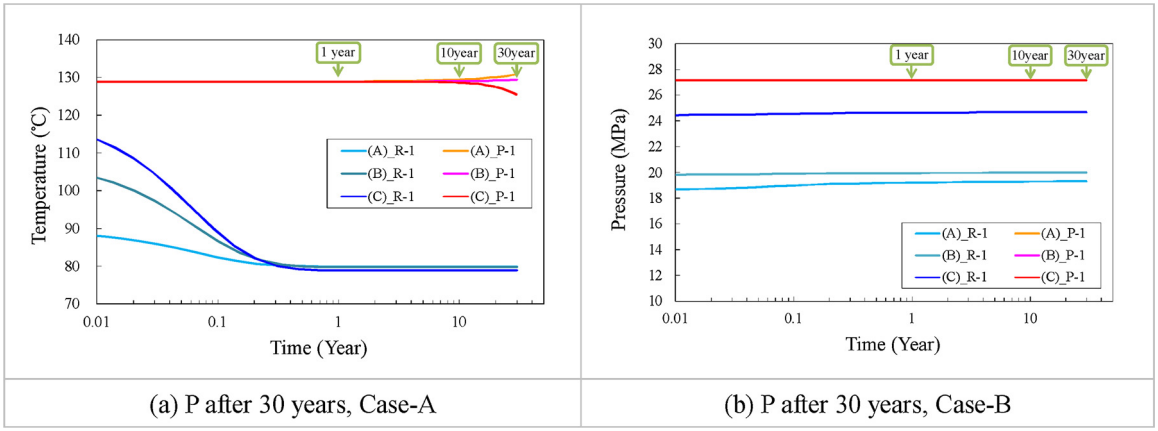

Fig. 14. P-T Evolutions during the 30-year Heat Production Period for All Cases.

4.4. Discussions

A basic production scenario analysis (BPSA) using the TOUGH2 code (coupled with a fit-for-purpose modified EGS module) as a relevant simulator was conducted for studying a potential geothermal site in Taiwan's I-lan Triangle. The simulation outcome shows the capability of the code can be comply with a heat production analysis under a pair of recharging and production wells.

By studying BPSA, locations of the recharging point from the production point are proven to be important to the adequate design of production well layout in a geothermal plant. Significant temperature decline can be observed in Case-C of BPSA, where the distance between R-1 and P-1 is the smallest among the 3 cases studied. In general, the water recharging into the production reservoir provides enough fluid which can prevent reservoir rock from drying out, but cares must be taken to minimize the temperature reduction due to the cool water mixing in the hot reservoir. From a geothermal engineering point of view, an optimum location from production point to recharging point can be allocated by using simulation tools with relevant reservoir structural and rock parameters.

In the results shown in Fig. 14, the temperature (T) change in the reservoir simulation (e.g., fixed state case) can be noted to exhibit a much more sensitive response than that of pressure (P) change. On a whole, the T conditions at R-1 exhibited significant changes with production time especially in the first production year when the reservoir structural condition and the location of recharging were varied. On the other hand, the production scenario analysis of Case-A, B, and C showed that the P conditions at P-1 would not change too much with a production time of 30 years.

When developing the modeling study for the BPSA Case, the initial guess of the geological structure model and corresponding rock parameters involved in the case was highly hypothetical and coming up with representative values was a very challenging task. Moreover, the exact same location and attitude of the D-fault is not well constrained. Although extensive on-site investigation has been carried out since 2014, together with many routine geothermal exploration approaches, including seismic reflection prospecting, magneto-tellurics (MT) survey, and conventional surface mapping, etc., all these methods were and will be conducted only on a regional scale under limited budget. Moreover, they can only provide limited clues to the reservoir properties regarding the actual geothermal structure model required for developing a realistic and site specific geothermal production model. Under such circumstances, owing to the complexity of the local geology and monotonic lithological change in the surveyed area, only a general conceptual model can be obtained.

It is fortunate that some pioneering exploration wells are under active planning and will be developed in upcoming years down to a depth of 1500–3000 mBGL, and the drilling results shall provide certain amount of on-site reservoir rock core samples and invaluable downhole pressure and temperature properties. The site specific geothermal production model, including the heat source characteristics, can be greatly improved when these data become available. Is addition, more precise boundary conditions can be taken to create more accurate heat production simulation results for future design.

Creating an EGS field is a long term goal in the I-lan area, and the reservoir heat production can be enhanced by reservoir stimulation using hydraulic fracturing technology. However, in Taiwan, there has been no real hands-on experience on such technology until today. However, future model studies should be conducted focusing on the impact of stimulation on the heat production efficiency.

5. Conclusions

By applying the TOUGH-EGS module, a basic production scenario analysis (BPSA) of the heat productivity was carried out to study a potential geothermal reservoir in Taiwan's I-lan area. Due to lack of a proven geological model, a conceptual reservoir model was constructed by using speculative models containing a major fault.

In the BPSA study, a numerical model for a hypothetical geothermal reservoir system was established associated with a production well and a recharging well. The recharging point was configured as Case-A, Case-B, and Case-C, according to their respective vertical distance from the production point, representing a base case EGS model. Heat production histories of target quartzite reservoirs were simulated using a deterministic approach, with model dimensions of 2 km × 2 km × 2.5 km taking into consideration a relevant boundary condition regarding Case-A, B, and C. The 30-year heat production P/T histories can be obtained, and the fault zone effect is evaluated. Significant temperature decline can be observed in Case-C of BPSA, where the distance between R-1 and P-1 is the smallest among the 3 cases studied.

In this study, a feasible production capacity estimation analysis procedure has been established. Competent simulation method is successfully created that can be applied to the site specific geothermal reservoirs in the I-lan area. Moreover, results of this study would provide a good example for formulating a T-H-M coupling simulation approach that hopefully can provide a useful numerical tool for future EGS development projects in Taiwan.

References

Chen, W.S., 2016. Technique Developments and Simulation of Enhanced Geothermal System in the I-lan Area. Final Progress Report of Geothermal Research Program, NEP Phase-II, Grant ID: NN10502-0140, Ministry of Science and Technology (MOST).

Department of Energy, 2008a. DOE Geothermal Technologies Program—Geothermal Tomorrow.

Department of Energy, 2008b. DOE Geothermal Technologies Program—An Evaluation of

Enhanced Geothermal Systems Technology.
Giardini, D., 2009. Geothermal quake risks must be faced. Nature 462 (7275), 848–849.
Goldstein, B., Hiriart, G., Bertani, R., Bromley, C., Gutierrez-Negrin, L., Huenges, E., Muraoka, H., Ragnarsson, A., Tester, J., Zui, V., 2011. Geothermal energy. In: Edenhofer, O., Pichs-Madruga, R., Sokona, Y., Seyboth, K., Matschoss, P., Kadner, S., Zwickel, T., Eickemeier, P., Hansen, G., Schlömer, S., von Stechow, C. (Eds.), IPCC Special Report on Renewable Energy Sources and Climate Change Mitigation. Cambridge University Press, Cambridge, United Kingdom and New York, NY, USA.
Ho, G.R., Chang, P.Y., Lo, W., Liu, C.M., Song, S.R., 2014. New evidence of regional geological structures inferred from reprocessing and resistivity data interpretation in the Chingshui-Sanshing-Hanchi Area of Southwestern Ilan County, NE, Taiwan. Terr. Atmos. Oceanic Sci. 25 (4), 491–504.
Hu, L.T., Winterfeld, P.H., Fakcharoenphol, P., Wu, Y.S., 2013. A novel fully-coupled flow and geomechanics model in enhanced geothermal reservoirs. J. Petrol. Sci. Eng. 107, 1–11.
International Geothermal Association, 2010. Geothermal a Natural Choice. IGA Geothermal Publication.
Jet Yen Company, 2012. Geothermal Power Generating in Sanshing Area within the I-lan Plain, A Developing Proposal of Geothermal Testing Plan Submitted to Bureau of Energy.
Lee, B.H., Guo, T.R., Lee, C.R., Liu, C.H., Ouyang, S., O'Sullivan, M.J., Yeh, A., 2012. 3D Numerical Modelling of Chingshui Geothermal Reservoir in Taiwan, Proceedings of the 2012 Australian Geothermal Energy Conference.
Lyu, Y.D., Tan, C.H., Yu, C.W., Chen, W.S., 2014a. In: Statistics and Analysis of Petrophysical Properties of Enhanced Geothermal Reservoirs, 2014 Taiwan Rock Engineering Symposium (2014 TRES). October 23–24, 2014 CYUT, Wufeng, Taichung, Taiwan.
Lyu, Y.D., Yu, C.W., Chen, W.S., 2014b. In: Simulation and Analysis of Heat Capacity of Enhanced Geothermal Reservoir, 2014 Taiwan Rock Engineering Symposium (2014 TRES). October 23–24, 2014 CYUT, Wufeng, Taichung, Taiwan.
Perapon, F., Xiong, Y., Hu, L., Winterfeld, P.H., Xu, T.F., Wu, Y.S., 2013. USER'S GUIDE of TOUGH2-EGS: A Coupled Geomechanical and Reactive Geochemical Simulator for Fluid and Heat Flow in Enhanced Geothermal Systems VERSION 1.0. Energy Modeling Group, Petroleum Engineering Department Colorado School of Mines May.
Pruess, K., 2005. ECO2N: A TOUGH2 Fluid Property Module for Mixtures of Water, NaCl, and CO2. Lawrence Berkeley Laboratory, Berkeley, CA August.
Pruess, K., Oldenburg, C., Moridis, G., 1999. Tough2 User's Guide, Version 2.0, Lawrence Berkeley National Laboratory Report LBNL-43134. Lawrence Berkeley Laboratory, Berkeley, CA November.
Teng, Louis, S.Y., Song, S.R., Yeh, E.C., Lin, A.T.S., Liu, C.M., Tsai, Y.L., 2013. Tectonic appraisal of geothermal potential of Taiwan. J. West. Pac. Earth Sci. 13 (December), 1–38.
Tester, J., Anderson, B.J., Batchelor, A.S., Blackwell, D.D., DiPippo, R., Drake, E.M., Garnish, J., Livesay, B., Moore, M.C., Nichols, K., Petty, S., Toksöz, M.N., Veatch, R.W., 2006. The Future of Geothermal Energy: Impact of Enhanced Geothermal Systems (EGS) on the United States in the 21 st Century. Massachusetts Institute of Technology.
Xu, T.F., Spycher, N., Sonnenthal, E., Zheng, L., Pruess, K., 2012. TOUGHREACT User's Guide: A Simulation Program for Non-isothermal Multiphase Reactive Transport in Variably Saturated Geologic Media, Version 2.0. Lawrence Berkeley Laboratory, Berkeley, CA October.
Yang, C.H., Yu, C.W., Lei, S.C., 2015. Laboratory Test of Fracture Permeability of Reservoir Rock from I-lan Geothermal Site, Proceedings of International Conference on Geothermal Energy (ICGE 2015) in Taiwan.
Yu, C.W., Lei, S.C., 2015. Innovative Development of Downhole Wire-line Fiber Optic Temperature-pressure Measuring System, Proceedings of International Conference on Geothermal Energy (ICGE 2015) in Taiwan.
Zhang, K., Lee, B.H., Ling, L., Wang, Y., Guo, T.R., Liu, C.H., Ouyang, S., 2016. Modeling studies for production potential of Chingshui geothermal reservoir. Renew. Energ. 94 (2016), 568–578.